CellPress

Neuron
Article

Translaminar Inhibitory Cells Recruited by Layer 6 Corticothalamic Neurons Suppress Visual Cortex

Dante S. Bortone,[1] Shawn R. Olsen,[1] and Massimo Scanziani[1,*]
[1]Howard Hughes Medical Institute, Center for Neural Circuits and Behavior, Neurobiology Section and Department of Neuroscience, University of California San Diego, La Jolla, CA 92093-0634, USA
*Correspondence: massimo@ucsd.edu
http://dx.doi.org/10.1016/j.neuron.2014.02.021

SUMMARY

In layer 6 (L6), a principal output layer of the mammalian cerebral cortex, a population of excitatory neurons defined by the NTSR1-Cre mouse line inhibit cortical responses to visual stimuli. Here we show that of the two major types of excitatory neurons existing in L6, the NTSR1-Cre line selectively targets those whose axons innervate both cortex and thalamus and not those whose axons remain within the cortex. These corticothalamic neurons mediate widespread inhibition across all cortical layers by recruiting fast-spiking inhibitory neurons whose cell body resides in deep cortical layers yet whose axons arborize throughout all layers. This study reveals a circuit by which L6 modulates cortical activity and identifies an inhibitory neuron able to regulate the strength of cortical responses throughout cortical depth.

INTRODUCTION

Layers are major subdivisions of cortical architecture whose identity is defined in terms of cell density, cellular specificity, afferent and efferent selectivity, molecular characteristics, and differences in their responses to sensory stimulation. Cortical layers are strongly interconnected through excitatory axonal projections (Binzegger et al., 2004; Callaway, 1998; Dantzker and Callaway, 2000; Douglas and Martin, 2004; Gilbert and Wiesel, 1979; Lefort et al., 2009; Lorente de No, 1922; Lund et al., 1979; Thomson and Bannister, 2003). Through these projections, it is believed that layers influence each other's activity (Gilbert and Wiesel, 1979; Hubel and Wiesel, 1962). Indeed, past and current work, using electrophysiological and pharmacological approaches, cooling methods, and more recently the combination of cell-specific Cre mouse lines with optogenetic tools, is beginning to reveal the functional impact that distinct layers have on one another (Adesnik and Scanziani, 2010; Beltramo et al., 2013; Constantinople and Bruno, 2013; Ferster and Lindström, 1985; Grieve and Sillito, 1991; Malpeli, 1983; Olsen et al., 2012; Schwark et al., 1986). This impact can be facilitatory (Adesnik and Scanziani, 2010; Beltramo et al., 2013; Schwark et al., 1986), suppressive (Olsen et al., 2012), mixed, or neutral (Constantinople and Bruno, 2013; Ferster and Lindström, 1985), yet still very little is known about the cellular mechanisms that mediate these interactions. Revealing the neuronal circuits orchestrating the interactions between layers is fundamental for our understanding of how these major subdivisions of cortical architecture contribute to information processing.

Layer 6 (L6) of the primary visual cortex (V1) has attracted the attention of many investigators because a large fraction of its pyramidal cells (PCs) project back to the thalamic nucleus from which V1 receives visual information, the dorsolateral geniculate nucleus (dLGN) (Bourassa and Deschênes, 1995; Jones, 2007; Thomson, 2010). Indeed, several studies have demonstrated that through this feedback projection, neurons in L6 can modulate the response of dLGN to visual stimuli (for reviews, see Briggs and Usrey, 2008; Guillery and Sherman, 2002; Sillito and Jones, 2002). L6 neurons, however, not only modulate dLGN activity but have also been shown to affect the response of the cortex to visual stimuli in both cats and rodents (Bolz and Gilbert, 1986; Grieve and Sillito, 1991; Olsen et al., 2012): pharamacological silencing of L6 facilitates visually evoked responses in more superficial layers (Bolz and Gilbert, 1986) (but see Grieve and Sillito, 1991). Furthermore, recent work taking advantage of the NTSR1-Cre mouse line, a line that targets a subpopulation of L6 PCs (L6PCs), demonstrated that optogenetic activation or silencing of this subpopulation leads to a suppression or facilitation, respectively, of visually evoked activity in more superficial layers (Olsen et al., 2012). Through its suppressive effect on visually evoked activity, L6 has been implicated in controlling gain and modulating size tuning during visual processing (Bolz and Gilbert, 1986; Olsen et al., 2012). Although it was long believed that L6's impact on cortical responses to sensory stimuli was mediated indirectly, via its action on the dLGN, electrophysiological evidence suggests that at least part of the suppressive effect of L6 on visually evoked cortical activity may actually be mediated directly, via intracortical projections (Bolz and Gilbert, 1986; Ferster and Lindström, 1985; Olsen et al., 2012). Furthermore, connectivity studies and anatomical data indicate the presence of circuit elements that could account for the intracortical suppression mediated by L6: L6PCs strongly innervate cortical inhibitory neurons (West et al., 2006) and inhibitory neurons in L6 have axons that can span several cortical layers (Kisvarday et al., 1987; Kumar and Ohana, 2008; Lund et al., 1988). If L6 indeed directly modulates cortical activity

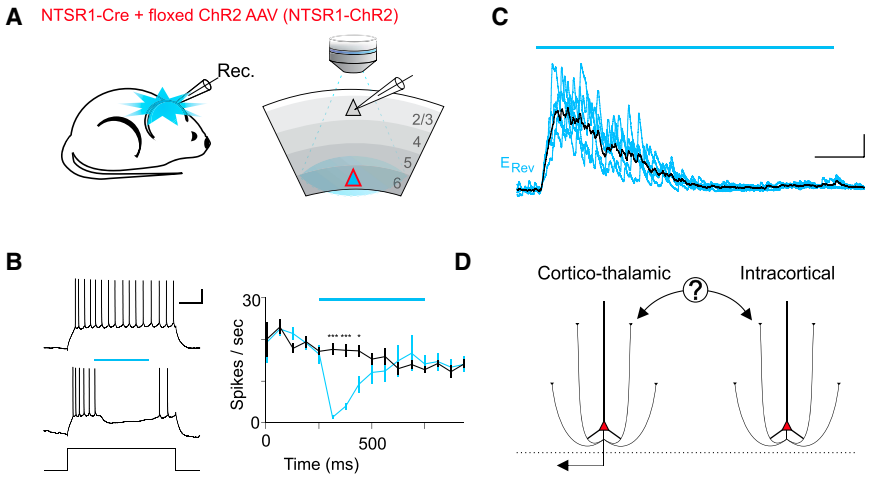

Figure 1. Photostimulation of NTSR1-Cre Neurons Suppresses Thalamus-Independent Cortical Activity In Vivo

(A) Illustration of in vivo recording configuration from V1 in an adult NTSR1-Cre mouse conditionally expressing ChR2. The ChR2-expressing layer 6 pyramidal cell (L6PC; red triangle) was photoactivated while recording from an L2/3 neuron (gray triangle).

(B) Left traces: response of an L2/3 neuron recorded in vivo in the whole-cell current-clamp configuration (scale bar, 200 pA 20 mV/250 ms) to current injection (150 pA; top) and to current injection with photoactivation of L6PCs (blue bar 0.5 s). Right: the average firing rate is plotted against time (black, control; blue, with photostimulation; asterisks indicate significant difference; p = 0.0002, 0.0002, 0.0074; n = 10 cells, 6 mice; blue bar, duration of photostimulation). Error bars represent SEM.

(C) IPSC recorded in vivo in an L2/3 neuron voltage clamped at +7 mV (scale bar, 200 pA/250 ms) in response to photoactivation of L6PCs (blue bar 1.5 s). Five superimposed sweeps (blue) are shown. Average trace is shown in black. See also Figure S1.

(D) Inhibition could be mediated by the activation of either corticothalamic or intracortical L6PCs.

independently of its impact on dLGN, what is the precise nature of the neural circuits through which it exerts its action? Answering this question is a crucial step in understanding the functional impact of a cortical layer based on the underlying cellular architecture. There are two large categories of L6PCs subdivided based on their axonal projections: intracortical L6PCs (L6ICs), whose axonal projections are restricted to the visual cortex, and corticothalamic L6PCs (L6CTs), which, in addition to cortical projections, also send an axonal collateral to the thalamus (Zhang and Deschênes, 1997). Which one of these two major classes of L6PCs is targeted by the NTSR1-Cre mouse line and thus contributes to the L6-mediated suppression of cortical activity, L6ICs or L6CTs? Furthermore, because L6PCs are excitatory, they cannot exert their cortical suppressive action without recruiting cortical GABAergic inhibitory neurons. What is the nature of the inhibitory neurons recruited by NTSR1-Cre neurons? Where are they located, and what are their morphological and physiological properties?

Here we show that in V1 the subpopulation of neurons targeted by the NTSR1-Cre line are all L6CTs and that the majority of L6CTs are targeted in the NTSR1-Cre line. Thus, L6CTs generate the suppression of cortical activity observed upon activation of neurons targeted by the NTSR1-Cre (Olsen et al., 2012). Although this suppression affects all cortical layers, it is mediated by the recruitment of inhibitory neurons whose cell bodies are located predominantly in L6. Widespread inhibition is achieved through a massive translaminar axonal arborization originating from these L6 inhibitory neurons and spanning throughout even the most superficial layers of the cortex. The identification of a circuit involving a large translaminar inhibitory neuron driven by L6CTs reveals a key mechanism by which L6 contributes to cortical sensory processing.

RESULTS

Optogenetic activation of neurons targeted by the NTSR1-Cre mouse line (from here on referred to as NTSR1 neurons) leads to a strong suppression of visually evoked activity in both dLGN and V1 (Olsen et al., 2012). Simultaneous extracellular recordings from these two structures suggest that at least part of the suppression of visually evoked activity in V1 is not indirectly due to the suppression of the dLGN (Olsen et al., 2012). If so, activation of NTSR1 neurons should also be able to suppress V1 activity that, unlike visually evoked activity, does not depend on dLGN input. We directly verified this possibility by performing in vivo whole-cell current-clamp recordings from V1 neurons in L2/3 (209 ± 13 μm deep, n = 10 cells, 6 mice) of anesthetized NTSR1-Cre mice (Gong et al., 2007; Olsen et al., 2012) that conditionally expressed Channelrhodopsin 2 (ChR2) (Boyden et al., 2005; Nagel et al., 2003) (Figure 1A). L2/3 neurons were depolarized with direct current injection above firing threshold (150–500 pA for 1 s) to trigger an average firing rate of 16.0 ± 1.1 Hz. Photostimulation of NTSR1 neurons (500 ms) strongly decreased this dLGN-independent firing of L2/3 neurons (8 of 10 cells were completely suppressed after 125 ms photostimulation; Figure 1B), consistent with the notion that NTSR1 neurons exert a powerful and direct suppression of cortical activity, independently of their impact on dLGN. Furthermore, consistent with a direct intracortical suppression, photostimulation revealed a large inhibitory postsynaptic current (IPSC) in layer L2/3 neurons recorded in vivo and voltage clamped at the reversal potential for synaptic excitation (~+7 mV; IPSC peak amplitude: 251.7 ± 68.2 pA; peak conductance: 3.1 ± 0.3 nS; n = 9 cells, 5 mice; recording depth 235.0 ± 16.1 μm; Figure 1C). In vitro pharmacology confirmed that this inhibition was disynaptic in all layers and therefore not the result of direct photostimulation of inhibitory neurons (Figure S1 available online). These results thus definitively validate the notion that NTSR1 neurons in L6 suppress cortical activity in vivo independently of their impact on the dLGN. These results however also open a fundamental question: what is the nature of the intracortical circuit through which NTSR1 neurons exert their suppressive action? This question is addressed below, first by establishing the type of L6PC whose activity leads to the observed cortical suppression and

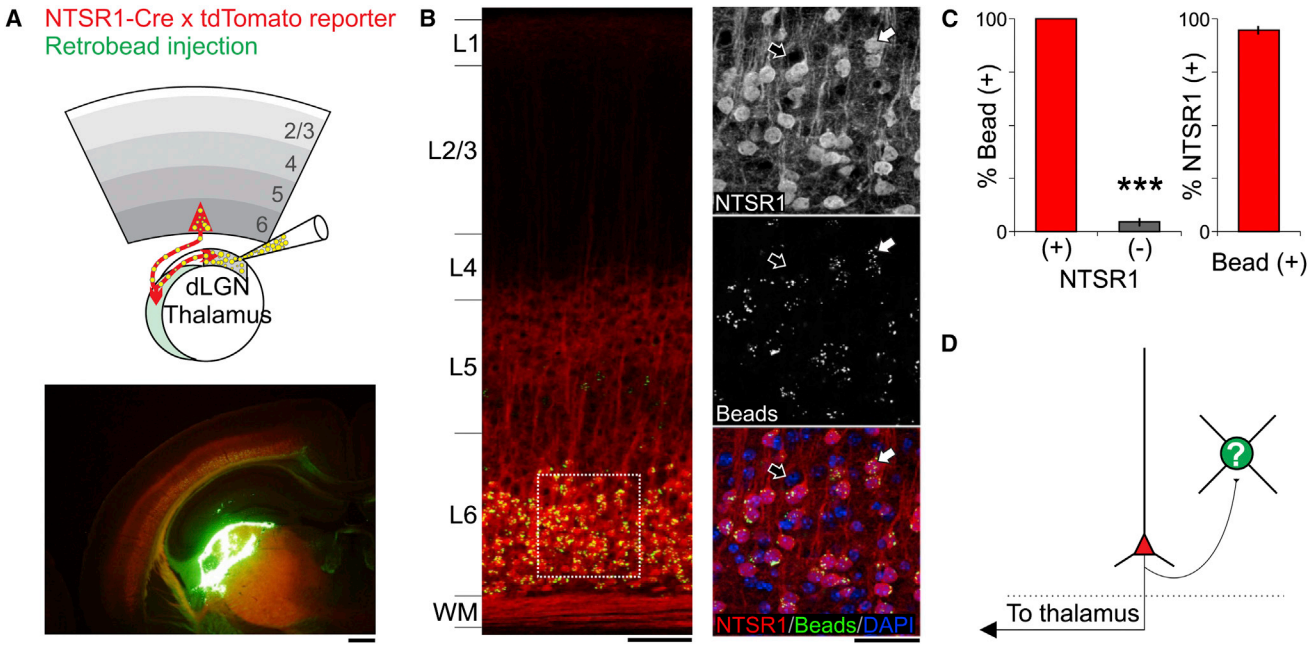

Figure 2. The NTSR1-Cre Line Selectively Targets Layer 6 Corticothalamic Pyramidal Cells

(A) Top left: schematic of thalamic injection of fluorescent microspheres into adult NTSR1-Cre X tdTomato reporter mouse in vivo. Green fluorescent microspheres are retrogradely transported to the soma of corticothalamic neurons. Bottom left: confocal image illustrating the thalamic injection site on a coronal section of the brain (red, tdTomato; green, fluorescent microspheres; yellow, superimposition of red and green; scale bar, 500 μm).

(B) Left: confocal image illustrating a coronal section through V1. Note the accumulation of microspheres in L6 (yellow fluorescence; scale bar, 100 μm). Right: magnification of area delineated by white square to left. Top right: red channel, confocal image of L6PCs expressing tdTomato (NTSR1+; scale bar, 50 μm; the white and black arrows indicate cell bodies that express or do not express tdTomato, respectively). Right middle: microspheres. Right bottom: overlay of red tdTomato expression, green microspheres, and blue nuclear counter stain (DAPI). Note that while all tdTomato-expressing cell bodies contained microspheres, most cell bodies lacking tdTomato expression do not contain beads.

(C) Summary histogram. Left: 154 of 154 tdTomato-expressing cells (red column; four mice) contained microspheres while only 9 of 197 nonexpressing cells contained microspheres (four mice; $p < 0.0001$). Right: 154 of 163 cells that contained microspheres expressed tdTomato (4 mice). Error bars represent SEM.

(D) What inhibitory interneurons are being recruited by L6CTs to suppress the visual cortex?

subsequently by revealing the cellular source of the observed cortical inhibition.

Which category of L6PC is responsible for the L6-mediated suppression of cortical activity, L6ICs or L6CTs (Zhang and Deschênes, 1997)? To answer this question, we determined which of these two L6PC categories are labeled by the NTSR1-Cre line used to drive the intracortical suppression. The strong axonal labeling in thalamic nuclei (including the dLGN, the nucleus reticularis thalami [nRT], and the and the mediorostral part of the lateral posterior thalamic nuclei [LPMR]) observed in sections from NTSR1-Cre brains conditionally expressing the tdTomato reporter (Olsen et al., 2012) suggests that at least some L6CTs are labeled by this line. To directly verify this possibility and, more importantly, to determine whether L6ICs are also labeled in the NTSR1-Cre line, we stereotactically injected fluorescent microspheres (RetroBeads, Lumafluor) in the dLGN and analyzed the distribution of RetroBeads in coronal sections of primary visual cortex 7–9 days after the injection (Figure 2). RetroBeads are taken up by axon terminals and retrogradely transported to the cell body. Thus, the presence of RetroBeads in the cell body of an L6PC identifies this cell as L6CT. We expected an underestimate of the actual percentage of corticothalamic neurons labeled by the line due to the unlikelihood that all axons that project to the dLGN pick up the beads. As such, we were surprised to find that all tdTomato-expressing L6PCs contained beads (100% ± 0%, n = 0/154 cells, 4 mice; Figures 2B and 2C). Furthermore, very few non-tdTomato-expressing L6PCs contained beads (4.7% ± 1.8%, n = 9/197 cells, 4 mice; Figures 2B and 2C). This finding not only validates the specificity of our bead-labeling method but also indicates that the NTSR1-Cre line is highly specific for driving expression in the L6CTs. Because Cre-expressing cells in the NTSR1-Cre line represent about 65% of the entire excitatory cell population in L6 (Olsen et al., 2012), these results also indicate that approximately 65% of L6 excitatory neurons in mouse V1 are L6CTs. Thus, these data demonstrate that of the two major categories of L6PCs in visual cortex, L6CTs are responsible for the intracortical suppression of cortical activity observed with the NTSR1-Cre line.

Through what inhibitory circuits do L6CTs operate to suppress cortical activity (Figure 2D)? We used linear probes to perform in vivo extracellular recordings throughout the depth of V1 in anesthetized NTSR1-Cre mice conditionally expressing ChR2 and photostimulated L6CTs. While the photostimulation suppressed the activity of most cortical neurons throughout layers, it also increased the firing of a small fraction of neurons

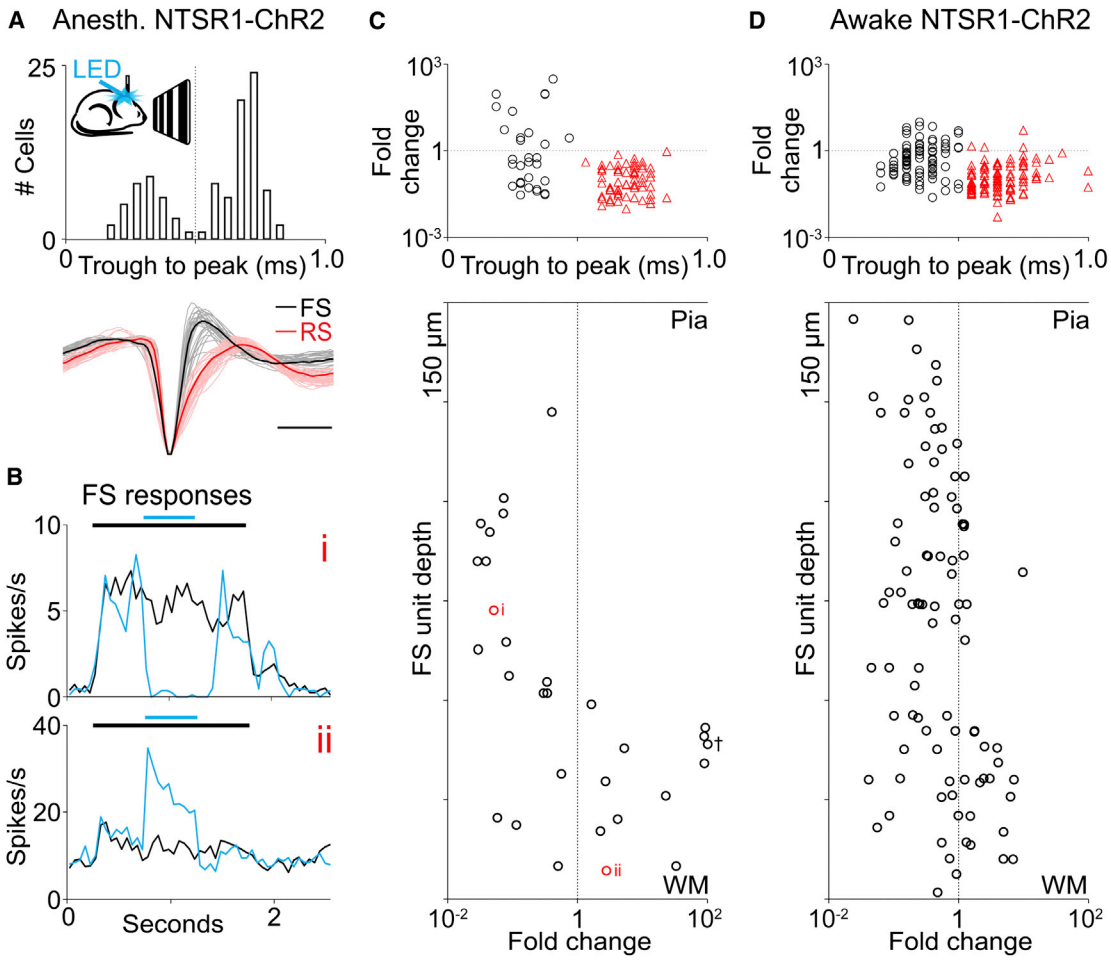

Figure 3. Selective Recruitment of Deep Layer Fast-Spiking Cells by Layer 6 Corticothalamic Pyramidal Cells In Vivo

(A) Schematic illustrates in vivo extracellular recording from V1 in NTSR1-ChR2 anesthetized mouse during visual stimulation and photoactivation of L6 corticothalamic pyramidal cells (L6CTs). Histogram shows separation of fast-spiking (FS) from regular spiking (RS) units based on trough-to-peak latency (102 units, 9 mice). Dotted line indicates the chosen divider for defining a unit as FS or RS. Bottom: 30 FS units (gray) and 30 RS units (pink) are shown on bottom with representative example shown in bold (scale bar, 0.5 ms).

(B) Peristimulus time histogram of the response of two example FS units to visual stimulation (black bar, 1.5 s) with (blue) and without (black) photoactivation of L6CTs (blue bar, 0.5 s). Note that while the top FS unit (i) is suppressed, the lower one (ii) is facilitated by photoactivation of L6CTs.

(C) Fold change in firing rate (LED on/LED off, log scale; black circles denotes FS units, red triangles RS units) in response to photoactivation of L6CTs during visual stimulation shown for all units in (A). Note that the only units whose firing rate increases during photoactivation of L6CTs are FS units. Recording depth of individual FS units are shown in bottom panel against the log scale of their fold change. Example units from (B) are labeled next to their corresponding depths (red circles). Cross indicates outlier moved from 296- to 100-fold change.

(D) In vivo unit recordings from awake mouse (n = 146 RS units 92 FS units; 4 mice) presented as in (C).

(11.7%, n = 12/102 cells, 9 mice; Figures 3A–3C; part of this data set [n = 90] was collected during a previous study [Olsen et al., 2012]). Interestingly, these neurons invariably showed fast-spiking (FS) properties, that is, their extracellularly recorded action potential had a fast time course with a trough-to-peak time less than 0.5 ms (0.31 ± 0.03 ms, n = 12, as compared with regular spiking neurons 0.69 ± 0.01 ms, n = 68). Such fast spikes represent the electrophysiological signature of a large category of GABAergic cortical inhibitory neurons that includes basket and chandelier cells. Importantly, not all recorded FS cells showed an increase in firing rate upon L6CT photostimulation (37.5%, n = 12/32 cells; Figures 3B and 3C). Where are the FS cells that increase their firing rate in response to L6CT photostimulation located? We determined the distribution of all extracellularly recorded FS cells across cortical depths. FS cells were distributed throughout the cortical radial axis yet, strikingly, those FS cells whose firing was increased upon photostimulation of L6CTs were selectively located in the deeper layers of the cortex. Specifically, from the pial surface to 600 µm deep 0% (n = 0/14 cells) of FS cells were recruited by L6CT activation, while below 600 µm 66.7% of FS units were recruited (n = 12/18 cells). Similar results were obtained when photostimulating L6CT in nonanesthetized animals (Figure 3D). A large fraction of FS cells below 600 µm was facilitated (45.9%; n = 17/37 cells,

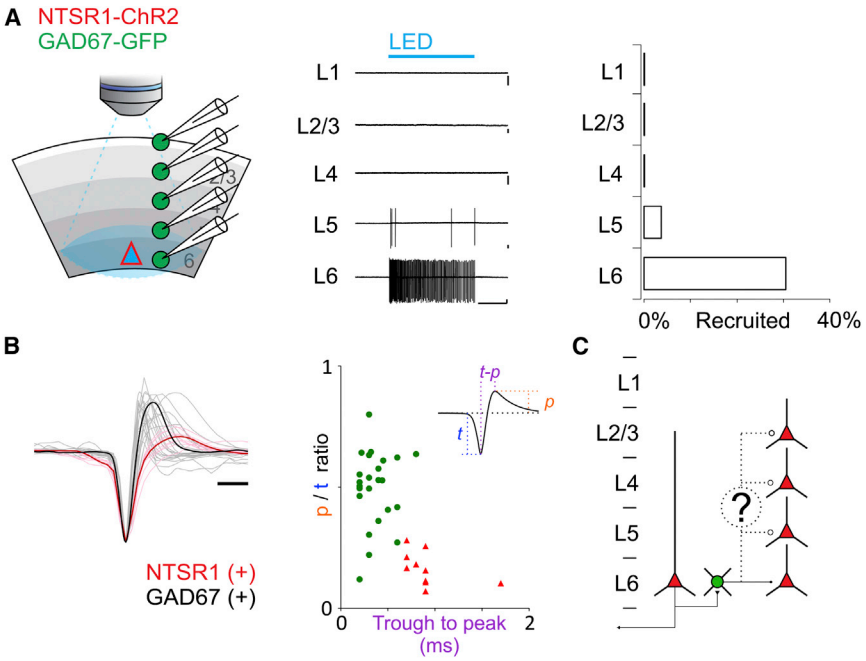

Figure 4. Selective Recruitment of Layer 6 Fast-Spiking Cells by Layer 6 Corticothalamic Pyramidal Cells In Vitro

(A) Left: schematic illustration of loose-patch recordings from GFP-expressing neurons in V1 slice from an NTSR1-ChR2 × GAD67-GFP mouse. A single loose-patch recording was made on a GFP-positive inhibitory neuron in L2/3, L4, L5, or L6 while photoactivating L6CTs. Center: example recordings from GFP-expressing neurons in each layer of one example slice during photoactivation of L6CTs (blue bar, 1.5 s). Note that only neurons in deeper layers fire in response to photoactivation (scale bars, 50 pA/500 ms). Right: summary histogram showing percentage of GFP-expressing neurons recruited by photoactivation of L6CTs (L1 n = 42, L2/3 n = 45, L4 n = 41, L5 n = 54, L6 n = 72; 7 mice). See also Figures S2 and S3.

(B) Left: waveforms of action potentials (average of first five spikes; recorded in loose patch) of all responding GFP-expressing neurons (GAD67(+); gray) and of directly photoactivated L6CTs (NTSR1(+); red, for comparison; scale bar, 0.5 ms). Bold lines shown are averages. Middle: peak-to-trough height ratio is plotted against trough-to-peak latency for GFP+ cells (green circles) and NTSR1+ cells (red triangles).

(C) Do L6 FS cells extend their axons throughout layers to inhibit also superficial neurons?

4 mice), while only 16.4% of all FS cells above 600 μm (n = 9/55 cells) increased their firing rate upon photostimulation of L6CT in nonanesthetized animals. Furthermore, the small fraction of FS cells above 600 μm whose firing rate was facilitated increased their firing rate significantly less than deeper FS cells (2.1 ± 0.9- and 3.4 ± 0.5-fold change, respectively; p = 0.0031). Consistent with these results, suppressing L6CT activity using the conditional expression of Arch/Halo in the NTSR1-Cre line significantly reduced the firing rate of most FS cells located below 600 μm (88.9%, p = 0.0392, n = 8/9 cells, 5 mice; average decrease 34.0% ± 11.7%). Together, these data indicate a preferential recruitment of FS cells in the deeper layers upon activation of L6CTs.

Is the recruitment of these deep FS cells responsible for the suppression of cortical activity throughout all cortical layers or is L6 photostimulation also recruiting additional cortical inhibitory neurons that are not detected by our recording electrodes? If our extracellular recordings do not provide an unbiased sample of the different types of inhibitory neurons present throughout cortical depth, recruited inhibitory neurons located in more superficial layers could have been missed.

To directly assess the distribution and type of cortical GABAergic neurons recruited by L6CTs, we performed recordings from visual cortex in vitro. Consistent with the in vivo data reported above, full-field photostimulation (1.5 s) of acute visual cortical slices from the NTSR1-Cre line conditionally expressing ChR2 generated large IPSCs in PCs cells throughout all layers (Figure S1). Therefore, as in vivo, in vitro photostimulation of L6CTs also generates widespread cortical inhibition. To identify the GABAergic neurons recruited by the activation of L6CTs, we crossed the NTSR1-Cre line with the GAD67-GFP line, a mouse line that expresses GFP in all GABAergic neurons (Tamamaki et al., 2003), and performed targeted loose-patch recordings from GFP-expressing cells (Figure 4A). Loose-patch recordings allow one to record the spiking activity of a neuron without perturbing its physiological cytosolic composition. Strikingly, while no GFP-expressing neuron in layers 1–4 (0 out of n = 128 cells, 7 mice) and only 3.7% (n = 2/54 cells) in L5 fired an action potential in response to photoactivation of L6CTs, almost a third (30.6%, n = 2/72 cells; Figure 4A) of L6 GFP-expressing neurons responded to the stimulus. Furthermore, the GFP-expressing neurons recruited by L6CTs had action potentials with FS waveforms (Figure 4B). Thus, the specific firing of FS cells in deeper layers in response to the activation of L6CTs is not due to a unit isolation bias of our in vivo recording configuration but represents a genuine selectivity in the recruitment of cortical inhibitory neurons by L6CTs. The preferential recruitment of inhibitory neuron in deep cortical layers was not due to the specific photostimulation protocol used here (a ramp of LED intensity; see Experimental Procedures). Photostimulating layer 6 with brief pulses of light (2 ms duration; see Experimental Procedures), also preferentially recruited inhibitory neurons in deeper layers (L1: 0%, n = 0/42; L2/3: 0%, n = 0/45; L4: 2%, n = 1/41; L5: 30%, n = 16/54; L6: 42%, n = 30/72; 7 mice; Figure S2). These data demonstrate that despite the widespread inhibition generated across cortical layers by activation of L6, the source of this inhibition appears to be mediated by GABAergic neurons whose somatic location is restricted to the deep cortical layers (Figure 4C).

By what mechanism do L6 corticothalamic neurons selectively recruit deep FS cells? We can hypothesize two extreme scenarios: in the first, L6CTs exclusively form synaptic contacts with FS cells located in deep layers; in the second scenario, L6CTs indiscriminately contact GABAegic cells throughout

cortical layers but only deep FS cells receive sufficiently strong synaptic input to be depolarized above action potential threshold. We tested these two scenarios by systematically performing whole-cell voltage-clamp recordings from GAD67-GFP-expressing neurons throughout cortical layers while photostimulating L6CTs in visual cortical slices. Consistent with the second scenario, all recorded GAD67-GFP-expressing neurons received direct excitation from L6CTs (n = 19 cells, 10 mice), indicating that they do not only contact deep-layer FS cells (Figure S3A). We thus tested whether recruited FS cells receive larger synaptic excitation from L6CTs as compared to the other contacted inhibitory neurons. We first identified GAD-EGFP-expressing neurons that fired in response to photostimulation of L6CTs. Consistent with the above results, these cells were invariably FS cells located in L6. We then compared the excitatory postsynaptic currents (EPSCs) evoked in these neurons with the EPSCs recorded in nonspiking GAD-EGFP-expressing neurons located either in L6 or in L2/3 of the same slice. Almost all GAD-EGFP-expressing neurons that fired in response to photostimulation of L6CTs received significantly larger EPSCs as compared to neighboring L6 or more distal L2/3 GABAergic neurons that did not fire (248.6 ± 50.8 pC L6 spiking versus 19.2 ± 5.7 pC nonspiking L2/3, n = 7 cells 5 mice, p = 0.0029; Figure S3B, left graph; and 317.1 ± 54.6 pC L6 spiking versus 84.8 ± 16.9 pC nonspiking L6, n = 6 cells 3 mice, p = 0.0155; Figure S3C, left graph). Furthermore, among recruited L6 FS cells, there was a significant correlation between the amount of excitatory charge received and the firing rate (p = 0.0008, n = 19 cells, 8 mice; Figure S3D, right). As a consequence of the larger excitation received by recruited L6 FS cells, the ratio between excitation and inhibition was also larger in these neurons (35.0% ± 6.0% L6 spiking versus 15.1% ± 3.1% nonspiking L2/3, n = 7, p = 0.0333; Figure S3B, right; and 42.1% ± 8.1% L6 spiking versus 21.7% ± 3.2% nonspiking L6, n = 6, p = 0.0396; Figure S3C, right). Thus, despite the fact that L6CTs contact inhibitory neurons throughout cortical layers, deep FS cells receive stronger excitation, a likely mechanism for their selective recruitment.

By what mechanism could deep FS cells generate inhibition throughout cortical layers? One possibility is that at least some of the cells recruited by corticothalamic L6PCs send an axonal projection that spans the entire cortical depth (Figure 4C). To test this hypothesis, we first identified GABAergic neurons that fired action potentials in response to L6CT photostimulation, using loose-patch recordings of GFP-expressing inhibitory neurons (see above and Experimental Procedures). We then obtained whole-cell current-clamp recordings from these neurons to determine their intrinsic membrane properties and to dialyze the neurons with an intracellular solution containing biocytin for subsequent morphological reconstruction. Initial anatomical reconstructions indicated the presence of at least two types of inhibitory neurons that were recruited by the activation of L6CTs: those whose axons arborized locally and remained confined within deep layers (Figure S4) and those that, consistent with our hypothesis, had axons that arborized throughout the entire cortical depth (Figure 5). We reconstructed the axonal arborization of 11 large translaminar neurons (9 mice) whose axonal arborization reached across all cortical layers containing excitatory neurons, from L6 to L2/3 (9 of 11 spanned from L6 to L1; Figure 5A). These 11 translaminar neurons were the result of filling 58 GFP-expressing interneurons or 19.0%. The average density of the axonal arborization peaked in L6 and L4, yet the exact distribution varied between neurons (Figure 5B). In contrast to the axonal arborization, the dendrites of these neurons were largely restricted to the deep cortical layers. Importantly, these dendrites lacked spines, consistent with the aspiny nature of cortical interneurons (Figure S5). Furthermore, consistent with in vivo and in vitro extracellular recordings, these large translaminar neurons showed properties typical of FS cells (Figure 6): high firing rates (66.0 ± 13.0 Hz; n = 11), little adaptation in response to current injections (16.9% ± 3.5%), pronounced afterhyperpolarization after every action potential (20.5 ± 0.7 mV, n = 10), and narrow action potentials (0.49 ± 0.06 ms, n = 11) with high peak-to-trough ratios (0.63 ± 0.04). While these characteristic FS properties were not significantly different between the two FS cell types recruited by L6CTs, i.e., between the translaminar and the local FS cells (Figures 6A and 6B), translaminar neurons reached significantly higher firing rates in response to L6CT photostimulation (99.7 ± 19.4 Hz translaminar interneurons versus 37.2 ± 11.7 Hz locally projecting, p = 0.0037).

Taken together, these results indicate that the activity of L6CTs can generate cortex-wide inhibition by recruiting FS cells whose soma is located in L6, yet whose translaminar axon spans all cortical layers (Figure 7).

DISCUSSION

Whether and how one of the major cortical outputs, the corticothalamic L6 pyramidal cells, directly impacts cortical function has been a long-standing question. While previous work of this and other labs provided evidence that L6PCs may directly suppress cortical activity (Bolz and Gilbert, 1986; Olsen et al., 2012), it was not clear whether this effect was due to L6ICs or L6CTs and how these PCs may mediate the suppression. By discovering that the NTSR1-Cre line selectively targets L6CTs, we have established that this cell type directly affects cortical excitability, independent of its thalamic projection. Furthermore, by identifying a large translaminar L6 FS cell whose axons span the entire cortical depth, we have revealed the mechanisms through which L6CTs exert their suppressive action on V1.

Through the present and previous work, we can now begin to understand the impact that L6CTs exert on their two main targets, the cortex and the thalamus: through their cortical projections, L6CTs provide excitation to most excitatory and inhibitory neurons across cortical layers; however, due to their particularly strong excitation of translaminar FS cells, the resulting disynaptic inhibition swamps the modest direct excitation mediated by L6CTs. These results are consistent with the report that L6CTs preferentially innervate cortical inhibitory neurons (West et al., 2006). Via their feedback projections to the thalamus, L6CTs target the nRT (the main inhibitory nucleus in the thalamus), the dLGN, and the LPMR. Because nRT neurons strongly inhibit dLGN neurons and because L6CT axons also innervate local inhibitory neurons in the dLGN, the overall impact of L6CTs onto dLGN relay neurons is, similar to cortex, suppressive (Olsen et al., 2012). The overall suppressive action of L6CTs on V1 and dLGN, however, should not be understood as a homogeneous

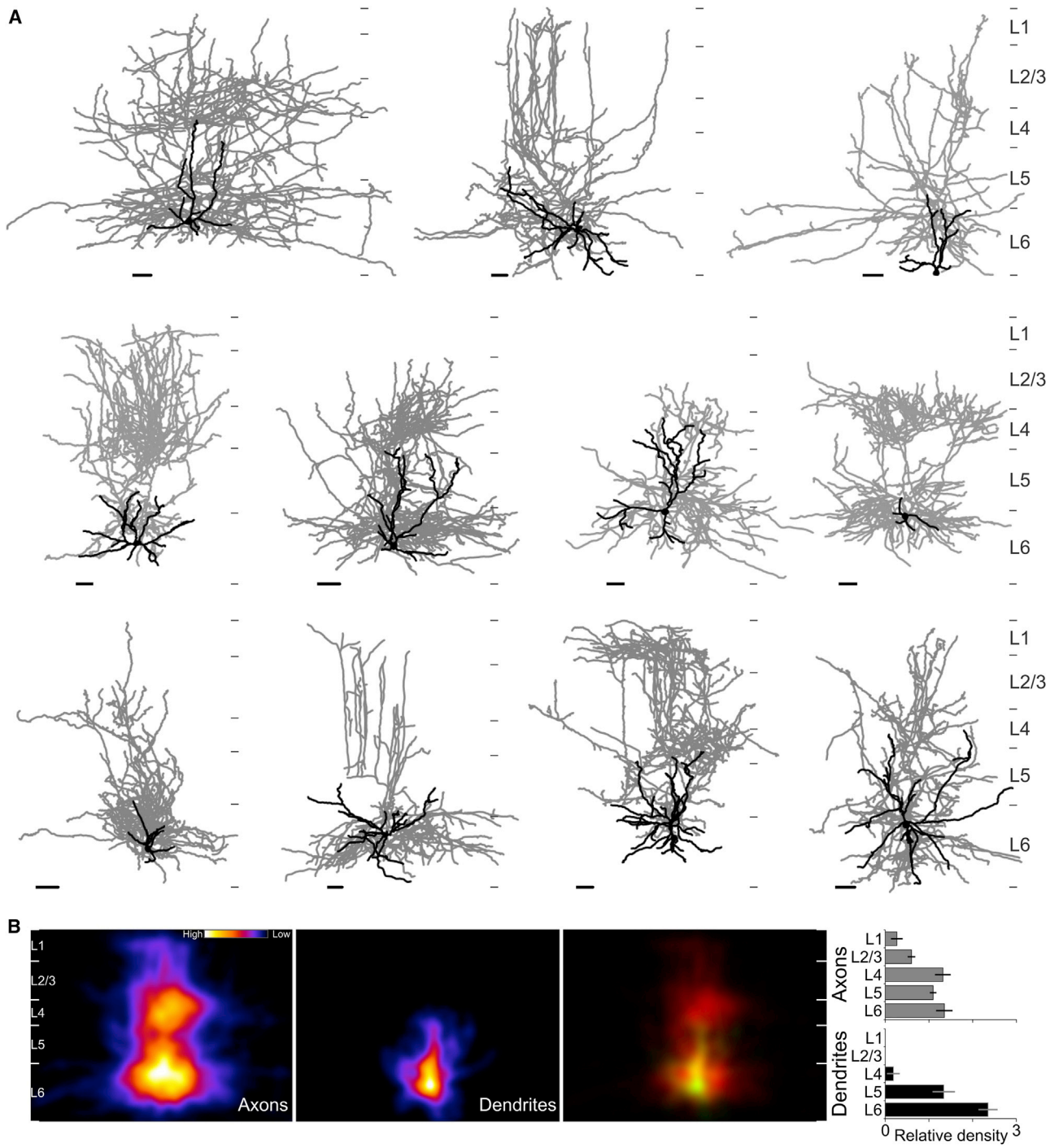

Figure 5. Translaminar Axonal Projections from Fast-Spiking Cells Recruited by Layer 6 Corticothalamic Pyramidal Cells

(A) Morphological reconstructions of 11 FS cells with translaminar axonal arborization that were recruited above threshold for spike generation upon photostimulation of L6CTs in vitro. Nine of the eleven translaminar FS cells were recorded in the GAD67-GFP line and expressed GFP. The remaining two FS cells (top row, first cell; bottom row, second cell) were recorded in the G42 line and also expressed GFP. Dendrites and somas are shown in black with axons in gray (scale bars, 50 μm; medial is to the right). Thin gray tics to right of each cell indicate layer boundaries.

(B) Average heatmap of axons (left) and dendrites (middle) of the 11 reconstructed translaminar FS cells after normalizing for differences in layer depths. Right: overlay of axons (red) and dendrites (colored green; yellow where overlapping with axons). Left: the relative density of neurite length for each layer for dendrites (black) and axons (gray) of all 11 cells. The relative density is the fraction of total neurite length divided by the fractional layer thickness; the fractional layer thickness is computed as the thickness of a layer divided by the cortical thickness, measured along the radial axis from the pia to the layer 6 white matter border. Error bars represent SEM.

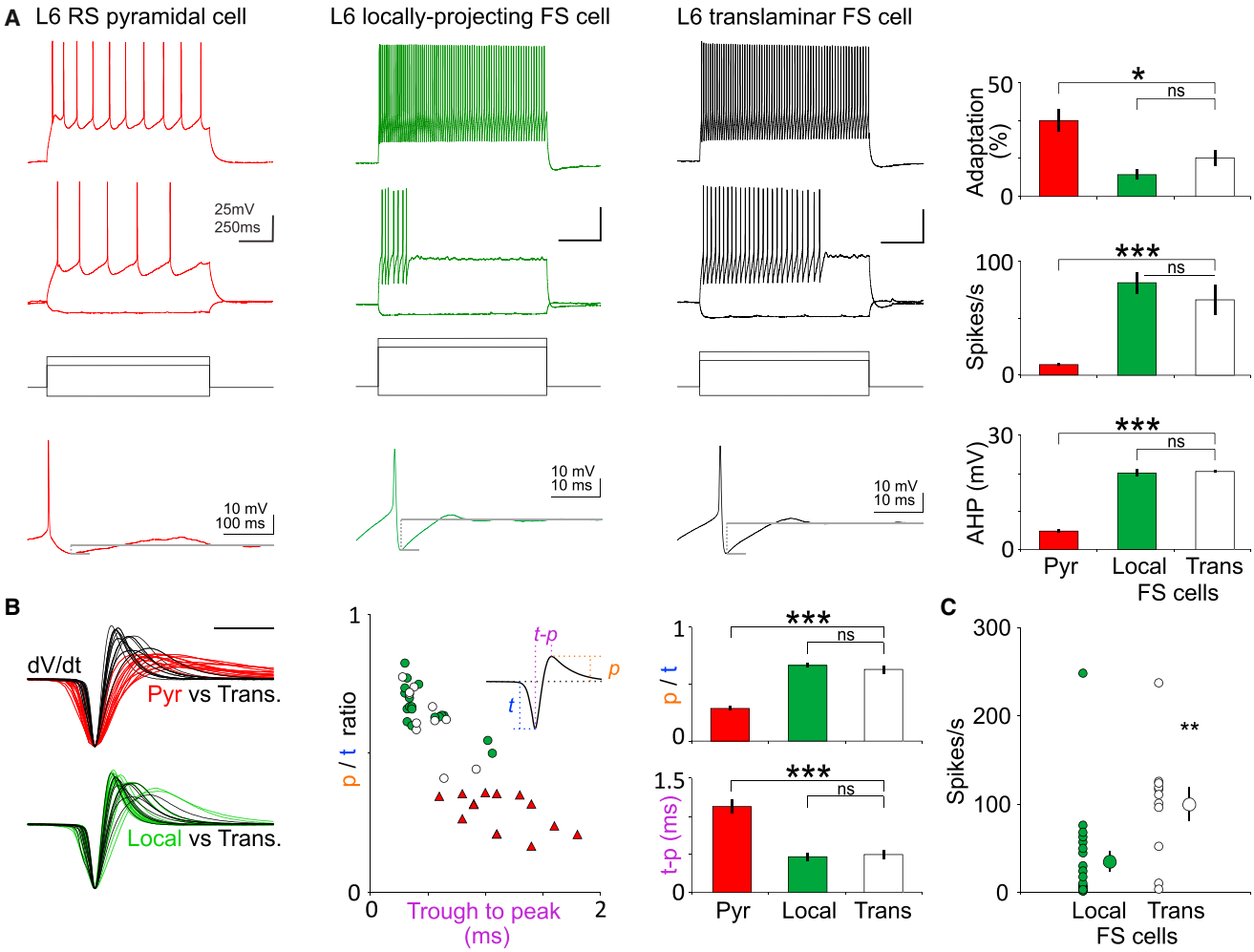

Figure 6. Electrophysiological Properties of Layer 6 Translaminar FS Cells

(A) Responses to steps of current injection are shown for L6CTs, locally projecting L6 FS cells, and translaminar FS cells. Translaminar FS cells (n = 11) did not significantly differ from locally projecting FS cells (n = 16) with respect to firing rate adaptation, firing rate, or afterhyperpolarization following an action potential (bottom traces), although they did significantly differ from regular spiking pyramidal cells (n = 10) in all these characteristics ($p = 0.0124$, $p < 0.0001$, and $p = 0.0002$, respectively; see Experimental Procedures for analysis parameters). Error bar represents SEM.

(B) Left: dV/dt of action potentials recorded in current clamp in translaminar FS cells (black traces; n = 11), L6CTs (red races; n = 13), and locally projecting FS cells (green traces; n = 16). Traces from translaminar FS cells are superimposed with those of L6CTs (top) and from locally projecting FS cells (bottom) for comparison. Center: the peak-to-trough ratio (p/t ratio) is plotted against the trough-to-peak latency of the dV/dt waveform (inset illustrates parameters measured, red triangle: RS pyramidal cell, green circle: locally projecting FS cell, open circle: translaminar FS cell). Right: averages and statistical comparison to right. No statistically significant difference was noted between locally projecting and translaminar FS cells. Translaminar FS cells did significantly differ from L6CTs in the peak-to-trough ratio ($p < 0.0001$) and in the trough-to-peak latency ($p = 0.0002$). Error bar represents SEM.

(C) Firing rate of FS cells in response to L6CT photoactivation: translaminar FS cells fired at significantly higher rates than locally projecting FS cells ($p = 0.0037$). Error bars represent SEM.

suppression of cortical and thalamic neurons. L6CTs provide direct excitation to PCs throughout all cortical layers and to dLGN relay neurons. If this excitation differs in its spatial distribution from that of the disynaptic inhibition generated by the recruitment of L6 FS cells, nRT cells, and local inhibitory neurons in the dLGN, neurons receiving direct excitation could be suppressed less than those receiving only disynaptic inhibition. In other words, the amount of suppression exerted by L6CTs in V1 and dLGN may have a spatial profile, reflecting the ratio of direct excitation and disynaptic inhibition received by each neuron (Murphy and Sillito, 1987). Furthermore, because of the disynaptic nature of inhibition, the onset of L6CT activity may transiently excite the target neurons before the onset of inhibition.

The L6 translaminar FS cell described here has no dendritic spines and expresses GFP in the GAD67-GFP mouse line, consistent with its hypothesized GABAergic nature. Furthermore, consistent with the strong correlation existing between FS cells and the expression of the protein parvalbumin (PV), we reconstructed two of the large translaminar FS cells

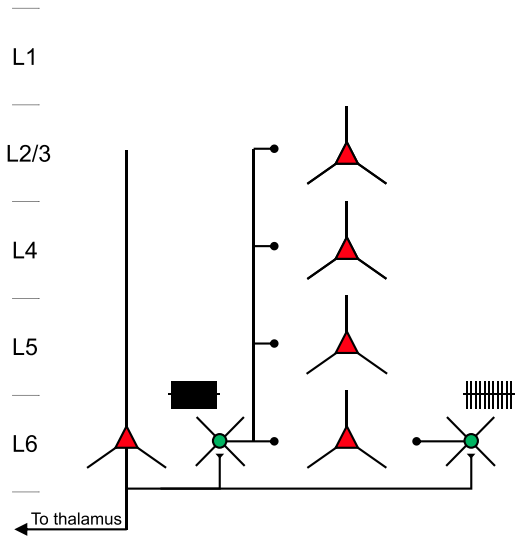

Figure 7. Model
L6CTs suppress responses in the visual cortex by recruiting FS cells located in L6, some of which extend large translaminar axon throughout all cortical layers.

from mice where the NTSR-1 Cre line was crossed with the G42 line, a mouse line that selectively labels PV-expressing, somatostatin-negative cells (Chattopadhyaya et al., 2004). The Martinotti cell is an anatomically, physiologically, and molecularly well described cortical inhibitory neuron whose axonal projection crosses layers to reach the most superficial ones (Markram et al., 2004; Wang et al., 2004). However, several properties of the translaminar FS cell described here distinguish it from Martinotti cells: the fast and nonadapting spike pattern, the complete lack of dendritic spines, and the GFP labeling in the G42 line, a line that excludes interneurons expressing somatostatin (Chattopadhyaya et al., 2004), a molecular marker of Martinotti cells (Kawaguchi and Kubota, 1996; Wang et al., 2004).

Approximately 20% of the FS cells recruited upon L6CT photostimulation and successfully reconstructed had a translaminar axonal arborization (Figure 5), while the rest had an axon that remained confined within the deep layers (Figure S4). While this percentage may reflect an actual prevalence of translaminar interneurons recruited by L6CTs, the proportion may be biased by our experimental protocols. A translaminar axon would be more likely to be cut than local axons. Additionally, the visually guided targeting of neurons may generate further biases, possibly leading to an enrichment or a reduction in our sampling of this population, for example, if the GFP expression is stronger or weaker, respectively, in translaminar as compared to other inhibitory neurons (Suzuki and Bekkers, 2010).

We attribute most of L6CT-mediated intracortical suppression of visually evoked activity in the superficial layers of V1 (Bolz and Gilbert, 1986; Olsen et al., 2012) to the recruitment of FS cells with translaminar axons. Additional mechanisms, however, cannot be ruled out: for example, if activity in L6IC facilitates the firing of PCs in superficial layers, the inhibition of L6ICs by FS cells whose axons are confined in the deep layers may contribute to the observed suppression.

The existence of non-Martinotti cortical inhibitory cells with translaminar axonal arborization is not novel in and of itself. In both supra- and infragranular layers, inhibitory neurons have been reported whose axonal arbors span several layers (Helmstaedter et al., 2009; Jiang et al., 2013; Kisvarday et al., 1987; Lorente de No, 1922; Lund, 1988; Somogyi and Cowey, 1981; Somogyi et al., 1981; Thomson and Bannister, 2003; Thomson et al., 2002). In particular, studies in rodents (Kumar and Ohana, 2008), carnivores (Kisvarday et al., 1987), and primates (Lund et al., 1988) have identified inhibitory neurons whose cell bodies are located in layer 6 and whose axons span several layers yet have morphological and physiological properties that differentiate them from Martinotti cells. Furthermore, a recent study (Buchanan et al., 2012) described an FS, PV-expressing L5 inhibitory neuron type that receives excitation from L5 PCs and whose ascending translaminar axonal arborization reaches L2/3. While the location of this L5 FS cell and the lack of axonal arborization in L1 distinguish it from the one we describe here, the translaminar L5 and L6 FS cells may represent a "family" of PV-expressing neurons with the ability of suppressing cortical activity across layers. Whether, like a Martinotti cell, translaminar FS cells also inhibit the dendritic compartment of PCs or whether, more like a PV-expressing FS basket cell, they inhibit the somatic and perisomatic compartments of PCs across cortical layers will be answered by additional anatomical work. The possibility of perisomatic inhibition mediated by translaminar axonal projections is well documented by work in cat visual cortex, where basket cells whose cell body is located in deep layers contact, through an ascending axonal arborization, the perisomatic compartment of PCs in more superficial layers (Kisvarday et al., 1987). Identifying molecular markers or combinations thereof that selectively label the L6 translaminar FS cells will be of great help for future anatomical and functional studies.

The results reported here also open new questions with regard to the function of L6. Do L6ICs differently impact cortical activity as compared to L6CTs? Do they also recruit the translaminar FS cells or do they exert their action through entirely distinct circuits? Furthermore, L6CTs labeled by the NTSR1-Cre line belong to two categories based on their dendritic arborization: those that send their dendrites to the most superficial layers and those whose apical dendrites end in L4 (Olsen et al., 2012), consistent with previous subdivisions of L6 pyramidal cells into tall and short (Briggs and Usrey, 2008). Do both of these L6CT types recruit the translaminar FS cells? Systematic electrophysiological paired recordings followed by morphological identification, the advent of new Cre lines selectively labeling L6ICs, or one of the two subtypes of L6CTs will provide the answer.

We have described an intracortical circuit by which L6CTs suppress V1. It would be of great interest to know whether other cortical layers, regions, or even other brain areas that send their projections to L6 also utilize this circuit to regulate the activity of V1.

EXPERIMENTAL PROCEDURES

All experiments were carried out in accordance with the animal care and handling guidelines set forth by the University of California.

Mouse Lines

The following mouse lines were used: NTSR1-Cre (strain B6.FVB(Cg)-Tg(Ntsr1-cre)GN220Gsat/Mmcd, stock number 030648-UCD), which was generated by the GENSAT project (Gong et al., 2007) and acquired from the Mutant Mouse Regional Resource Centers; tdTomato reporter (Hongkui Zeng, Jax number 007908); GAD67-GFP (Δneo, Takeshi Kaneko); and G42 GAD67-GFP (Z. Josh Huang, Jax number 007677).

In Vivo Anesthetized Extracellular Recordings

In vivo multichannel silicon probe recordings were conducted as previously described (Olsen et al., 2012). Briefly, mice were anesthetized with 5 mg/kg chlorprothixene, and 1.2 g/kg urethane. We used 0.5%–1.0% isoflurane during surgery. A head plate was mounted over V1 and the skull was thinned using a dental drill. PBS was then applied to the thinned skull and sharpened forceps were then used to make a hole large enough to allow the insertion of the NeuroNexus 16-channel linear probe (A1x16-3mm-50-177). The probe was inserted at a depth of 800–1,000 μm, which was estimated based on the depth and angle of the probe insertion. PBS was then applied to keep the craniotomy moist. After more than 20 min of probe insertion, visual stimuli were presented using a gamma-corrected, Dell 52 × 32.5 cm LCD monitor (60 Hz refresh rate, mean luminance 50 cd/m^2, 25 cm from contralateral eye). Full-field sinusoidal drifting gratings (2 Hz, 0.04 cycles per degree, 100% contrast) were generated using Psychophysics ToolBox (Brainard, 1997). The visual stimulus was 1.5 s with a 3–6 s intertrial interval during which a gray screen was presented. Visual stimulus trials were interleaved with trials presenting both visual stimulus and a 0.5 s 20 mW LED pulse (470 nm, 1 mm diameter, Doric Lenses). Black foil (Thor Labs) was used to prevent the LED from reaching the eyes. Recordings were amplified ×1,000 and band-pass filtered between 0.3 Hz and 5 kHz using an AM systems 3500. Acquisition was done at 32 kHz with a NIDAQ PCIe-6239 board using custom MATLAB software (MathWorks).

In Vivo Awake Extracellular Recordings

Five to seven days before recording, head plates were implanted over V1. Isoflurane (2.5%) was used during the implantation procedure. The skin was removed and the head plate was fixed in place with black dental cement. Kwik-Cast (WPI) was then used to cover the skull. Animals were injected with 0.1 mg/kg buprenorphine subcutaneously and monitored daily.

Prior to recording, mice were familiarized to head fixation for three 10 min daily sessions. During these training sessions, the head plate was clamped to a metal post allowing mice to run on a plastic circular treadmill (Fast-Trac from Bio-Serv).

For recordings, mice were anesthetized using 1.5%–2% isoflurane. A small craniotomy was then made over V1, a drop of PBS was placed in the well of a head plate that was clamped to a metal post, and a NeuroNexus 32-channel linear probe (A1x32-Edge-5mm-20-177) was inserted into the craniotomy. A higher channel probe was used in the awake mouse because of the desire to use as few mice as possible for these experiments and technological improvements. Mice were given at least 30 min to recover from anesthesia before recordings began. Recording sessions were between 1 and 2 hr long. Acquisition was done at 20 kHz to accommodate higher channel density.

Solutions

Sucrose solution contained 83 mM NaCl, 2.5 mM KCl, 3.3 mM $MgSO_4$, 1 mM NaH_2PO_4, 26.2 mM $NaHCO_3$, 22 mM d-glucose, 72 mM sucrose, and 0.5 mM $CaCl_2$, bubbled with 95% O_2 and 5% CO_2. Artificial cerebrospinal fluid (ACSF) contained 119 mM NaCl, 2.5 mM KCl, 1.3 mM NaH_2PO_4, 26 mM $NaHCO_3$, 20 mM d-glucose, 1.3 mM $MgCl_2$, 2.5 mM $CaCl_2$, and 305 mM mOsm, bubbled with 95% O_2 and 5% CO_2. Cesium-based internal solution 125 mM $CsMeSO_4$, 4 mM NaCl, 10 mM HEPES, 0.3 mM Na_3GTP, 4 mM MgATP, 0.3 mM EGTA, 2.5 mM QX-314-Cl, 10 mM BAPTA(5Cs), adjusted to pH 7.4 with CsOH (140 ml; mOsm 295). Potassium-based internal solution contained 150 mM K-gluconate, 1.5 mM $MgCl_2$, 5 mM HEPES, 1.1 mM EGTA, 10 mM phosphocreatine, adjusted to pH 7.4 with KOH, 295 mM mOsm. HEPES-buffered ACSF contained 142 mM NaCl, 5 mM KCl, 10 mM HEPES sodium salt, 10 mM d-glucose, 1.3 mM $MgCl_2$, and 3.1 mM $CaCl_2$, carbogen free.

In Vivo Whole-Cell Recordings

Mice (5 to 10 weeks old) were anesthetized using chlorprothixene (5 mg/kg mouse) and isoflurane (1%–2.5%). Dexamethazone (0.5 μl/g mouse) was given to reduce swelling. The head was fixed to a mounting plate using dental cement (Lang Dental Manufactoring). A dremmel was used to thin the entire skull covering V1 and to make a small craniotomy (approximately 250 μm diameter). The dura was removed and the craniotomy was covered with HEPES-buffered ACSF. Recordings were obtained using the blind patch technique (Margrie et al., 2002). Cortical depth was determined by using the angle and depth of insertion of the recording pipette. The depth boundaries of L2/3 were chosen by measuring the depth of the layer in slices of primary visual cortex (134 ± 7.8 μm to 333 ± 15.2 μm, n = 6 mice). Conservative boundaries of 150–300 μm were chosen based on these depth measurements. Pipettes (4–6 MΩ tip resistance) filled with either cesium or potassium-based internals (see solutions) were quickly advanced to a cortical depth of 150 μm with a positive pressure of 3 psi. A 100 Hz train of 5 mV steps were applied to continuously measure the resistance of the pipette tip. Positive pressure was reduced to 0.5 psi as the pipette was advanced in steps of 2 μm through the depth of L2/3. Upon advancing, a sharp increase in pipette resistance accompanied with the appearance of an oscillation was taken as an indication of contact with the cell. Pressure was removed to obtain a GΩ seal. Neurons were voltage clamped at the reversal potential of inhibition (−73.5 mV with cesium internal solution) to record EPSCs. To record IPSCs, we voltage clamped neurons at the reversal potential of excitation (approximately +7 mV with cesium internal solution).

Data were acquired as in in vitro slice preparation.

In Vitro Slice Preparation and Recordings

Mice (4 to 8 weeks old) were anesthetized using ketamine (100 mg/kg) and xylazine (10 mg/kg). The descending aorta was clamped and right atrium cut before perfusing 1 min with chilled sucrose solution. Coronal sections of V1 (300 μm, Bregma −2.2 to −4) were made using a vibratome (DSK Microslicer DTK-1000) in a chilled sucrose solution. Slices were incubated in sucrose solution in a submerged chamber at 34°C for 45 min and then at room temperature (21°C) until used for recordings. Whole-cell recordings were done at 31.5°C in ACSF using pipettes with 3–5 MΩ resistance. Excitatory and inhibitory synaptic currents were recorded using a cesium-based internal solution. Whole-cell current-clamp recordings to monitor spiking activity were performed using a potassium-based internal solution. Loose-patch recordings were performed using ACSF as an internal (>8 MΩ seal). Biocytin-filled cells included 0.2%–0.5% biocytin in the internal solution. Filled cells were held for 10–20 min and immediately fixed in 4% PFA in PBS. A Vector ABC kit was used to process filled neurons, which were then traced using Neurolucida. Data were recorded with Multiclamp 700B amplifiers (Axon Instruments). Current-clamp recordings were filtered at 10 kHz and digitized with a Digidata1440A (Axon Instruments) at 50 kHz. Voltage-clamp recordings were filtered at 3 kHz and digitized at 10 kHz. Axon binary files were imported to Igor Pro (Wavemetrics) using DataAccess (Bruxton) and analyzed using custom-made routines. Charges represent the time integral of the synaptic current recorded during the first second of photostimulation. The stage was moved using a custom plugin for ImageJ (NIH) to interface with ESP300 (Newport) via SerialPort (SerialIO). Drugs used were NBQX (10 μM; Tocris 1044) and CPP (20 μM; Ascent Asc-159).

Retrograde Labeling

Green RetroBeads IX were injected as received from Lumafluor into 4-week-old mice. Mice were anesthetized with isofluorane (1%–2.5%) and a small craniotomy was made with a dremmel. To label corticothalamic neurons, we injected green retrobeads into the dLGN (coordinates: 2 mm posterior from bregma, 2 mm lateral from midline, at a depth of 2.9–3 mm) of 4-week-old mice using a stereotactic apparatus. Beads (350 nl) were injected bilaterally at a rate of 50 nl/min.

Viral Injections and Photostimulation

Adeno-associated viruses (AAVs) for ChR2 were acquired from the University of Pennsylvania Viral Vector Core: AAV2/1.CAGGS.flex.ChR2.tdTomato. SV40. ChR2 virus was injected into newborn pups (between postnatal days

0 and 2) that were anesthetized on ice. Each animal was virally injected at three locations in V1 along the mediolateral axis. At each location the virus was injected at two depths (550 μm and 650 μm; 13.2 nl/depth). For extracellular recordings the photostimulus consisted of a 0.5 s 20 mW pulse delivered by an LED coupled to a fiber optic (470 nm, 1 mm diameter, Doric Lenses). Photostimulation of L6 during whole-cell and loose-patch recordings consisted of either 7.5 mW/cm^2 pulses of 2 ms duration or of ramps of increasing intensity (in vitro: 0 to 0.54 mW/cm^2; in vivo: 0 to 7.5 mW/cm^2; ramp duration: 1.5 s except in Figure 1B where a shorter protocol was given [0.5 s] to avoid excessive spike accommodation) using a 470 nm wavelength LED (LEDC5 Thor Labs) through a GFP filter cube (GFP-3035B-OMF-ZERO, Semrock BrightLine) and a 40× water-immersion objective.

Data Analysis

Whole-Cell Recordings

Inhibitory and excitatory charges were computed as the time integral of the IPSC or EPSC, respectively. The integral began at the start of L6CT photoactivation and lasted for 1 s. Adaptation was calculated as $1 - \mathrm{Freq}_{AVE}/\mathrm{Freq}_{INIT}$, where Freq_{AVE} was the average instantaneous frequency over the entire current injection and Freq_{INIT} was the average instantaneous frequency for the first 100 ms of the current step injection. The current injection used for the measurement of adaptation and firing rate (Figure 6A) was the lowest current injection able to induce firing for the entire duration of the 1 s step. Afterhyperpolarization was calculated on sweeps where the current injection was enough to elicit spikes but not for the entire duration of the current injection so a baseline could be determined. Spike waveforms used were an average of the first five recorded spikes. The peak-to-trough ratio was obtained by dividing the absolute value at the peak (second deflection) by the absolute value of the trough (first deflection).

Extracellular Recordings

Data were analyzed with custom-written software using MATLAB. Single units were isolated using software provided by D.N. Hill, S.B. Mehta, and D. Kleinfeld (Fee et al., 1996). Signals were high-pass filtered at 500 Hz and waveforms were extracted from four adjacent electrode sites. Spikes were defined as events exceeding 4–5 SD of the noise. Waveforms were clustered using a k-means algorithm and further aligned using a graphical user interface. Fisher linear discriminant analysis and refractory period violations were used to assess unit isolation quality. Units were assigned a depth based on the channel in which they showed the strongest signal.

RetroBeads

For quantification of beads in corticothalmic neurons, a confocal stack of images was made of layer 6. A stereotactic plane was drawn the centermost image (200 μm medial lateral, L6 dorsal ventral). Included cells were those whose somas touched this plane without touching the bottom and left boundaries. The entire soma (as shown by either the reporter expression or the absence of labeling) was required to be in the stack of images to be included in counting. Cells whose soma included beads were designated corticothalamic.

Statistics

Error bars in all figures represent SEM. Statistical analysis was done using VassarStats (http://www.vassarstats.net). Mann-Whitney test was used for Figures 1B, 3D, and 6A–6C. Paired t test was used for Figures S3B and S3C and for Arch/Halo extracellular recordings mentioned in the text. Fisher's test was used for Figure 2B. Linear correlation and regression used for Figure S3D.

Axonal and Dendritic Density

Heatmaps of reconstructed interneurons were done by normalizing the size of each neuron by the total cortical depth and converting Neuroleucida reconstructions into bitmap images using Adobe Illustrator. Then, the following bitmap manipulations were done using ImageJ (NIH): to allow mapping of layers onto one another, the neurites in each layer were stretched or shrunk along the dorsal ventral axis to the match same dorsal ventral dimension across different slices. Cells bodies were aligned in the medial lateral axis. Bitmap images were Gaussian filtered to a radius of 50 pixels (approximately 35 μm). The contrast of each cell's Gaussian filtered image was adjusted to make the highest pixel intensity for the image the maximum value possible before averaging the images for each cell type. These group average images were again adjusted for contrast to make the highest pixel intensity for the image the maximum value possible. The color look-up table used was ImageJ's "Fire."

SUPPLEMENTAL INFORMATION

Supplemental Information includes five figures and can be found with this article online at http://dx.doi.org/10.1016/j.neuron.2014.02.021.

ACKNOWLEDGMENTS

We wish to thank J. Isaacson, J. Reynolds, our reviewers, and the members of the Scanziani and Isaacson laboratories for helpful discussions of this project; J. Evora for DAB biocytin processing, mouse colony maintenance, and administrative support; M. Chan and A. Linder for neonatal viral injections; the Gene Expression Nervous System Atlas (GENSAT) Project, NINDS Contracts N01NS02331 and HHSN271200723701C to The Rockefeller University (New York, NY); the UCSD Neuroscience Microscopy Facility (P30 NS047101) for the use of their imaging equipment; and R. Lowry and Vassar College for the statistical analysis tools. D.S.B. is supported by Ruth L. Kirschstein NRSA (1F32NS076185-01A1). M.S. is an investigator of the Howard Hughes Medical Institute. This work was also supported National Institutes of Health grant RO1 NS069010 and by the Gatsby Charitable Foundation.

Accepted: February 8, 2014
Published: March 20, 2014

REFERENCES

Adesnik, H., and Scanziani, M. (2010). Lateral competition for cortical space by layer-specific horizontal circuits. Nature *464*, 1155–1160.

Beltramo, R., D'Urso, G., Dal Maschio, M., Farisello, P., Bovetti, S., Clovis, Y., Lassi, G., Tucci, V., De Pietri Tonelli, D., and Fellin, T. (2013). Layer-specific excitatory circuits differentially control recurrent network dynamics in the neocortex. Nat. Neurosci. *16*, 227–234.

Binzegger, T., Douglas, R.J., and Martin, K.A. (2004). A quantitative map of the circuit of cat primary visual cortex. J. Neurosci. *24*, 8441–8453.

Bolz, J., and Gilbert, C.D. (1986). Generation of end-inhibition in the visual cortex via interlaminar connections. Nature *320*, 362–365.

Bourassa, J., and Deschênes, M. (1995). Corticothalamic projections from the primary visual cortex in rats: a single fiber study using biocytin as an anterograde tracer. Neuroscience *66*, 253–263.

Boyden, E.S., Zhang, F., Bamberg, E., Nagel, G., and Deisseroth, K. (2005). Millisecond-timescale, genetically targeted optical control of neural activity. Nat. Neurosci. *8*, 1263–1268.

Brainard, D.H. (1997). The Psychophysics Toolbox. Spat. Vis. *10*, 433–436.

Briggs, F., and Usrey, W.M. (2008). Emerging views of corticothalamic function. Curr. Opin. Neurobiol. *18*, 403–407.

Buchanan, K.A., Blackman, A.V., Moreau, A.W., Elgar, D., Costa, R.P., Lalanne, T., Tudor Jones, A.A., Oyrer, J., and Sjöström, P.J. (2012). Target-specific expression of presynaptic NMDA receptors in neocortical microcircuits. Neuron *75*, 451–466.

Callaway, E.M. (1998). Local circuits in primary visual cortex of the macaque monkey. Annu. Rev. Neurosci. *21*, 47–74.

Chattopadhyaya, B., Di Cristo, G., Higashiyama, H., Knott, G.W., Kuhlman, S.J., Welker, E., and Huang, Z.J. (2004). Experience and activity-dependent maturation of perisomatic GABAergic innervation in primary visual cortex during a postnatal critical period. J. Neurosci. *24*, 9598–9611.

Constantinople, C.M., and Bruno, R.M. (2013). Deep cortical layers are activated directly by thalamus. Science *340*, 1591–1594.

Dantzker, J.L., and Callaway, E.M. (2000). Laminar sources of synaptic input to cortical inhibitory interneurons and pyramidal neurons. Nat. Neurosci. *3*, 701–707.

Douglas, R.J., and Martin, K.A. (2004). Neuronal circuits of the neocortex. Annu. Rev. Neurosci. *27*, 419–451.

Fee, M.S., Mitra, P.P., and Kleinfeld, D. (1996). Automatic sorting of multiple unit neuronal signals in the presence of anisotropic and non-Gaussian variability. J. Neurosci. Methods *69*, 175–188.

Ferster, D., and Lindström, S. (1985). Synaptic excitation of neurones in area 17 of the cat by intracortical axon collaterals of cortico-geniculate cells. J. Physiol. *367*, 233–252.

Gilbert, C.D., and Wiesel, T.N. (1979). Morphology and intracortical projections of functionally characterised neurones in the cat visual cortex. Nature *280*, 120–125.

Gong, S., Doughty, M., Harbaugh, C.R., Cummins, A., Hatten, M.E., Heintz, N., and Gerfen, C.R. (2007). Targeting Cre recombinase to specific neuron populations with bacterial artificial chromosome constructs. J. Neurosci. *27*, 9817–9823.

Grieve, K.L., and Sillito, A.M. (1991). A re-appraisal of the role of layer VI of the visual cortex in the generation of cortical end inhibition. Exp. Brain Res. *87*, 521–529.

Guillery, R.W., and Sherman, S.M. (2002). Thalamic relay functions and their role in corticocortical communication: generalizations from the visual system. Neuron *33*, 163–175.

Helmstaedter, M., Sakmann, B., and Feldmeyer, D. (2009). Neuronal correlates of local, lateral, and translaminar inhibition with reference to cortical columns. Cereb. Cortex *19*, 926–937.

Hubel, D.H., and Wiesel, T.N. (1962). Receptive fields, binocular interaction and functional architecture in the cat's visual cortex. J. Physiol. *160*, 106–154.

Jiang, X., Wang, G., Lee, A.J., Stornetta, R.L., and Zhu, J.J. (2013). The organization of two new cortical interneuronal circuits. Nat. Neurosci. *16*, 210–218.

Jones, E.G. (2007). The Thalamus, Second Edition. (Cambridge: Cambridge University Press).

Kawaguchi, Y., and Kubota, Y. (1996). Physiological and morphological identification of somatostatin- or vasoactive intestinal polypeptide-containing cells among GABAergic cell subtypes in rat frontal cortex. J. Neurosci. *16*, 2701–2715.

Kisvarday, Z.F., Martin, K.A., Friedlander, M.J., and Somogyi, P. (1987). Evidence for interlaminar inhibitory circuits in the striate cortex of the cat. J. Comp. Neurol. *260*, 1–19.

Kumar, P., and Ohana, O. (2008). Inter- and intralaminar subcircuits of excitatory and inhibitory neurons in layer 6a of the rat barrel cortex. J. Neurophysiol. *100*, 1909–1922.

Lefort, S., Tomm, C., Floyd Sarria, J.C., and Petersen, C.C. (2009). The excitatory neuronal network of the C2 barrel column in mouse primary somatosensory cortex. Neuron *61*, 301–316.

Lorente de No, R. (1922). La corteza cerebral de raton. Trabajos del Laboratorio de Investigaciones Biologicas de la Universidad de Madrid *20*, 41–78.

Lund, J.S. (1988). Anatomical organization of macaque monkey striate visual cortex. Annu. Rev. Neurosci. *11*, 253–288.

Lund, J.S., Henry, G.H., MacQueen, C.L., and Harvey, A.R. (1979). Anatomical organization of the primary visual cortex (area 17) of the cat. A comparison with area 17 of the macaque monkey. J. Comp. Neurol. *184*, 599–618.

Lund, J.S., Hawken, M.J., and Parker, A.J. (1988). Local circuit neurons of macaque monkey striate cortex: II. Neurons of laminae 5B and 6. J. Comp. Neurol. *276*, 1–29.

Malpeli, J.G. (1983). Activity of cells in area 17 of the cat in absence of input from layer a of lateral geniculate nucleus. J. Neurophysiol. *49*, 595–610.

Margrie, T.W., Brecht, M., and Sakmann, B. (2002). In vivo, low-resistance, whole-cell recordings from neurons in the anaesthetized and awake mammalian brain. Pflugers Arch. *444*, 491–498.

Markram, H., Toledo-Rodriguez, M., Wang, Y., Gupta, A., Silberberg, G., and Wu, C. (2004). Interneurons of the neocortical inhibitory system. Nat. Rev. Neurosci. *5*, 793–807.

Murphy, P.C., and Sillito, A.M. (1987). Corticofugal feedback influences the generation of length tuning in the visual pathway. Nature *329*, 727–729.

Nagel, G., Szellas, T., Huhn, W., Kateriya, S., Adeishvili, N., Berthold, P., Ollig, D., Hegemann, P., and Bamberg, E. (2003). Channelrhodopsin-2, a directly light-gated cation-selective membrane channel. Proc. Natl. Acad. Sci. USA *100*, 13940–13945.

Olsen, S.R., Bortone, D.S., Adesnik, H., and Scanziani, M. (2012). Gain control by layer six in cortical circuits of vision. Nature *483*, 47–52.

Schwark, H.D., Malpeli, J.G., Weyand, T.G., and Lee, C. (1986). Cat area 17. II. Response properties of infragranular layer neurons in the absence of supragranular layer activity. J. Neurophysiol. *56*, 1074–1087.

Sillito, A.M., and Jones, H.E. (2002). Corticothalamic interactions in the transfer of visual information. Philos. Trans. R. Soc. Lond. B Biol. Sci. *357*, 1739–1752.

Somogyi, P., and Cowey, A. (1981). Combined Golgi and electron microscopic study on the synapses formed by double bouquet cells in the visual cortex of the cat and monkey. J. Comp. Neurol. *195*, 547–566.

Somogyi, P., Cowey, A., Halász, N., and Freund, T.F. (1981). Vertical organization of neurones accumulating 3H-GABA in visual cortex of rhesus monkey. Nature *294*, 761–763.

Suzuki, N., and Bekkers, J.M. (2010). Inhibitory neurons in the anterior piriform cortex of the mouse: classification using molecular markers. J. Comp. Neurol. *518*, 1670–1687.

Tamamaki, N., Yanagawa, Y., Tomioka, R., Miyazaki, J., Obata, K., and Kaneko, T. (2003). Green fluorescent protein expression and colocalization with calretinin, parvalbumin, and somatostatin in the GAD67-GFP knock-in mouse. J. Comp. Neurol. *467*, 60–79.

Thomson, A.M. (2010). Neocortical layer 6, a review. Front. Neuroanat. *4*, 13.

Thomson, A.M., and Bannister, A.P. (2003). Interlaminar connections in the neocortex. Cereb. Cortex *13*, 5–14.

Thomson, A.M., West, D.C., Wang, Y., and Bannister, A.P. (2002). Synaptic connections and small circuits involving excitatory and inhibitory neurons in layers 2-5 of adult rat and cat neocortex: triple intracellular recordings and biocytin labelling in vitro. Cereb. Cortex *12*, 936–953.

Wang, Y., Toledo-Rodriguez, M., Gupta, A., Wu, C., Silberberg, G., Luo, J., and Markram, H. (2004). Anatomical, physiological and molecular properties of Martinotti cells in the somatosensory cortex of the juvenile rat. J. Physiol. *561*, 65–90.

West, D.C., Mercer, A., Kirchhecker, S., Morris, O.T., and Thomson, A.M. (2006). Layer 6 cortico-thalamic pyramidal cells preferentially innervate interneurons and generate facilitating EPSPs. Cereb. Cortex *16*, 200–211.

Zhang, Z.W., and Deschênes, M. (1997). Intracortical axonal projections of lamina VI cells of the primary somatosensory cortex in the rat: a single-cell labeling study. J. Neurosci. *17*, 6365–6379.